Published in final edited form as:
Neurosci Res. 2012 January ; 72(1): 32–42. doi:10.1016/j.neures.2011.10.002.

Demyelination and remyelination in anatomically distinct regions of the corpus callosum following cuprizone intoxication

Andrew J. Steelman, **Jeffrey P. Thompson**, and **Jianrong Li**‡
Department of Veterinary Integrative BioSciences, Texas A&M University, College Station, Texas, USA 77843

Abstract

Multiple sclerosis is a chronic demyelinating disease of the central nervous system. Spontaneous remyelination during early disease stages is thought to preserve and partially restore function. However, this process ceases in later stages despite the presence of pre-oligodendrocytes. Cuprizone-induced demyelination is a useful model with which to study the remyelination process. Previous studies have demonstrated heterogeneities in demyelination in individual animals. Here we investigated regional differences in demyelination and remyelination within the corpus callosum. C57BL/6 mice were fed 0.2% cuprizone for 5 weeks to induce demyelination. Remyelination was examined 2–5 weeks after cuprizone withdrawal. Immunohistochemistry and electron microscopy were used to quantify regional differences in demyelination, gliosis, and remyelination. We found that, while demyelination was limited in the rostral region of corpus callosum, nearly complete demyelination occurred in the caudal callosum, beginning at approximately −0.5 mm from bregma. Astrogliosis and microgliosis were correlated with demyelination and differed between the rostral and caudal callosal structures. Remyelination upon cessation of cuprizone ensued at different rates with splenium remyelinating faster than dorsal hippocampal commissure. Our data show anatomical differences of cuprizone-induced demyelination and remyelination in the corpus callosum and the importance of examining specific callosal regions in myelin repair studies using this model.

Introduction

Multiple sclerosis (MS) is a devastating disease of the central nervous system (CNS) that almost always results in debilitation. Demyelination and inflammation are pathological hallmarks of MS and are both thought to contribute to axon injury, and the eventual cerebral atrophy that is prevalent in the later stages of the disease (Compston and Coles, 2008). Pathologically, MS lesions have been categorized into four distinct patterns (I-IV) based on complement activation, IgG deposition, and preferential loss of myelin associated glycoprotein (Lucchinetti et al., 2000). Of these four, pattern III lesions are distinguished from others by displaying extensive macrophage/microglia activation, accompanied by oligodendrocyte apoptosis, and are consistent with a “dying back” gliopathy caused by hypoxia, metabolic stress or viral infection (Lucchinetti et al., 2000). While still under

‡Corresponding author: Jianrong Li, Ph.D., Department of Veterinary Integrative Biosciences, Texas A&M University, Mail Stop 4458, College Station, TX 77843, Phone: 979-862-7155, Fax: 979-847-8981, jrli@cvm.tamu.edu.

The authors have no conflict of interest to declare.

debate, some evidence suggests that this particular pathology may constitute one of the initial events in lesion formation (Barnett and Prineas, 2004; Breij et al., 2008; Lucchinetti et al., 2000).

Continued ingestion of the copper chelator cuprizone (bis-cyclohexanone-oxaldihydrazone) results in a white matter pathology that is similar to pattern III MS lesions, and thus has proven to be a useful model with which to study the pathogenesis of primary demyelination caused by mitochondrial dysfunction (Liu et al., 2010; Lucchinetti et al., 2000; Pasquini et al., 2007; Suzuki and Kikkawa, 1969). As in other animal models, the degree of demyelination depends on mouse strain (Skripuletz et al., 2008; Taylor et al., 2009; Taylor et al., 2010), anatomic location (Gudi et al., 2009; Stidworthy et al., 2003a), age (Kipp et al., 2009), dose (Hiremath et al., 1998), and gender (Taylor et al., 2009). However, the pathology following cuprizone intoxication of C57BL/6 mice is well characterized and highly reproducible. In this model, mice fed cuprizone for 3 weeks exhibit extensive reactive gliosis accompanied by oligodendrocyte apoptosis. Demyelination is evident after 4–6 weeks of intoxication in multiple structures including the hippocampus (Koutsoudaki et al., 2009), external capsule (Pott et al., 2009), rostral cerebellar peduncles (Blakemore, 1973; Ludwin, 1978), cerebellum (Groebe et al., 2009; Skripuletz et al., 2010), striatum (Pott et al., 2009), cerebral cortex (Gudi et al., 2009; Skripuletz et al., 2008) and most notably the corpus callosum (Matsushima and Morell, 2001). Although the exact mechanism underlying cuprizone-induced demyelination remains to be elucidated, it is thought to result from unrelenting mitochondrial stress brought on by the toxic effects of the drug itself in conjunction with the effector functions of the innate immune response (Linares et al., 2006; Liu et al., 2010; Pasquini et al., 2007). Interestingly, a spontaneous remyelination process begins at the height of demyelination, and is greatly potentiated upon the removal of the toxin with nearly complete remyelination in a matter of weeks (Blakemore, 1972; Matsushima and Morell, 2001). As remyelination protects against neurodegeneration and promotes functional recovery (Bando et al., 2008; Duncan et al., 2009; Irvine and Blakemore, 2008), many studies have utilized the cuprizone model, in conjunction with other toxin-induced demyelination models, to investigate the molecular events pertinent to remyelination (Arnett et al., 2001; Mi et al., 2009; Plant et al., 2005). In these studies the dependency on consistent demyelination of anatomical structures in the brain, most notably the corpus callosum, is paramount to making accurate and meaningful comparisons.

To date several studies have demonstrated anatomical differences in the extent of demyelination within the corpus callosum of individual cuprizone-fed mice (Stidworthy et al., 2003a; Wu et al., 2008; Xie et al., 2010). However, detailed analysis of demyelination in different anatomical regions of the corpus callosum is incomplete as most have divided the corpus callosum into three equally spaced regions rather than its known physiologically relevant five: the lamina rostralis, genu, body, isthmus and splenium. In addition, the dorsal hippocampal commissure, a separate anatomic structure, has often been included in the caudal analysis of the splenium. Precise mapping of anatomical locations of demyelination within the corpus callosum will provide valuable insight for the design of studies aimed at promoting remyelination, especially those involving stereotaxic injection of potential therapeutics. Here, we report marked differences in the degree of demyelination, astrogliosis, and microgliosis in the brains of C57BL/6 mice fed 0.2% cuprizone for five weeks. Demyelination is anatomically distinct within the corpus callosum with the caudal region most susceptible. Importantly, upon toxin withdrawal remyelination ensues more quickly in the splenium when compared to the dorsal hippocampal commissure. Our findings stress the importance of examining myelin integrity and extent of gliosis at specific anatomical regions of corpus callosum when making comparisons among various experimental groups using the mouse cuprizone model.

Materials and Methods

Animals and cuprizone administration

Male C57BL/6 aged 7 weeks were received from Harlan and allowed 1 week to acclimate to their new environment prior to the onset of the experiment. Cuprizone (Sigma, C9012) was milled into normal mouse chow at a concentration of 0.2% and formed into standard pellets at Harlan (Harlan, TD.01453). Age-matched control mice were kept on a normal diet. Mice in experimental groups were fed for a total of 5 weeks to induce demyelination. Food pellets were changed every other day. After 5 weeks post-cuprizone feeding, the diet was changed to normal rodent chow for additional 2 and 5 weeks to examine remyelination. Mice were housed two animals per cage and weights and food intake were examined daily. Both food and water were provided *ad libitum*. All cuprizone chow was stored in vacuum sealed containers at 4°C until use. All animal protocols adhered to NIH Guidelines for Care and Use of Laboratory Animals and were approved by the Texas A&M University Laboratory Care and Use Committee.

Tissue processing

For histological and immunohistochemical analysis, mice were anesthetized by i.p. injection of xylazine/ketamine, and fixed by transcardial perfusion using 20 ml of sterile PBS followed by 20 ml of 4.0% paraformaldehyde (PFA) in PBS at a rate of 2 ml/min. using a Fusion 100 syringe pump (Chemyx Inc., Stafford, TX). The brains were removed and post-fixed overnight at 4°C in PFA then cryoprotected with 30% sucrose in PBS. The brains were segmented in either coronal or sagittal planes with the aid of a mouse-specific alto 0.5 mm stainless steel matrix (Roboz Surgical Instrument Company, Inc. Gaithersburg, MD), then frozen with dry ice. Coronal and sagittal sections of 20 μm thickness were cut using a microtome, placed on glass slides and stored at −80°C.

Myelin staining and demyelination scoring

Myelin was visualized by oil red O staining. Briefly, sections were rehydrated with distilled water for 5 min. and treated with 100% propylene glycol (Poly Scientific; Bay Shore, NY) for 2 min., then soaked in oil red O (Poly Scientific; Bay Shore, NY) for 24–48 hours. Excess stain was removed by washing the slides with 85% propylene glycol followed by a wash with distilled water. Sections were then lightly stained with hematoxylin (Vector; Burlingame, CA) to visualize nuclei.

The extent of demyelination in both coronal and sagittal sections was determined by two investigators blinded to animal treatment. The distance of demyelination from bregma in sagittal and coronal sections was assessed according to the third edition of The Mouse Brain: In Stereotaxic Coordinates by Franklin & Paxinos (Franklin and Paxinos, 2008). Percent demyelination was subjectively scored by 2 independent investigators as follows: demyelination ranging from 0 – 10 % of the total anatomical structure was scored as a 0; 10 – 30 % represented a score of 1; 31 – 60 % represented a score of 2; 61 – 90% represented a score of 3; and 91 – 100% of demyelination represented a score of 4 (Supplemental Fig. 1). Image Processing and Analysis in Java (Image J) software was also used to score demyelination in sagittal sections. Five areas of interest in the corpus callosum were selected to best represent the variations in demyelination with respect to anatomic location from bregma. Starting with the most rostral portion of the corpus callosum these areas were: 1.34 to 1.14 mm, 0.6 to 0.4 mm, −0.2 to −0.4 mm, −0.8 to −1 mm, and −2.2 to −2.4 mm from bregma, corresponding to the genu (gcc), body (bcc), isthmus (icc), and two representing the splenium corpus callosum (scc), respectively. Image J was used to measure these distances in a sagittal view of the brain. Specifically, we measured the distance to said areas of interest using the most rostral tip of the corpus callosum as a known structural reference. We then

drew a box (200 μm^2) around that region of the corpus callosum and scored the demyelination within that boxed region. When available, scores of multiple coronal sections (2–3) within each area of interest were averaged. The final score from each region represents the average scores from each group of mice.

Immunohistochemistry and immunofluorescence

Myelin basic protein (MBP), microglia, astrocytes and mature oligodendrocytes were revealed by immunohistochemistry using both diaminobenzidine (DAB) and immunofluorescence utilizing antibodies specific for MBP, ionized calcium binding adaptor molecule-1 (Iba-1), glial fibrillary acidic protein (GFAP), and glutathione-S transferase isoform pi (GST-π) antigens respectively. For DAB staining, samples were rehydrated with TBS, then treated with 1% H_2O_2 (Fluka analytical). The samples were blocked and permeabilized with TBS containing 0.1% Triton-X and 5% goat serum. Primary antibodies were applied overnight, diluted in TBS as indicated below. Anti-GFAP (1:100, rabbit IgG; Zymed) was used to visualize astrocytes, anti-GST-π (1:500, rabbit IgG; Assay Designs) was used to visualize mature oligodendrocytes, anti-Iba1 (1:500, rabbit IgG; Wako) was used to visualize microglia/macrophages, anti-neurofilament (1:100, rabbit IgG; Millipore) was used to visualize axons, anti-NG2 (1:150, Chemicon) was used to visualize progenitor cells and anti-SMI32 (1:200, Covance) was used to visualize axonal spheroids. The secondary antibody (anti-rabbit, IgG, biotinylated) was obtained from Vectastain and used at a dilution of 1:200. All reagents used to develop the stain were obtained from the Peroxidase Rabbit IgG kit (Vectastain) and used as stated by the manufacturer. For immunofluorescent staining samples were rehydrated, blocked, permeabilized and treated with primary antibodies as described above. All secondary antibodies were purchased from Invitrogen and diluted to a concentration of 1:1000 in blocking solution and were incubated for 1h at room temperature.

Analysis of fluorescence intensity and cell counting

Fluorescent intensity of GFAP and Iba-1 immunostaining was used as a semi-quantitative measure of astrogliosis and microgliosis respectively. All images were acquired using an Olympus DP70 digital camera mounted on an Olympus IX71 microscope. Images from both coronal and sagittal sections corresponding to 0.6 to 0.4 mm from bregma as well as −0.8 to −1.0 mm from bregma were taken using a 40X objective. All pictures were acquired using the same intensity and exposure time. Background was uniformly subtracted from each image using the eyedropper tool in Adobe Photoshop. Fluorescent intensity was then measured using Image J. Changes in fold intensity were calculated by dividing the intensity of each mouse by the average intensity of control mice for each specific anatomical location. To determine $GFAP^+$ and Iba-1^+ cell numbers, the mono-colored images used for intensity measurement were first merged with Hoechst staining and then analyzed by counting nucleated $GFAP^+$ or Iba-1^+ cells in each field. Axonal spheroids in the corpus callosum and dorsal hippocampal commissure were determined by counting the number of $SMI32^+$ spheroids in multiple 40× fields (3 per section, 2 sections per mouse, n=5). Data were expressed as cells per mm^2.

Transmission electron microscopy (TEM)

In a subset of mice, demyelination and remyelination of the corpus callosum were examined and compared at the ultrastructural level by TEM. Mice were anesthetized and perfused as described above with PBS and then fixed with 20 ml PBS containing 2% paraformaldehyde and 2.5% glutaraldehyde (Electron Microscopy Sciences, Hatflield PA) and post-fixed overnight at 4°C. The brains were then segmented in the medial sagittal plane with the aid of a mouse-specific alto 0.5 mm stainless steel matrix (Roboz Surgical Instrument Company, Inc. Gaithersburg, MD), trimmed to 2–3 mm thick segments and washed in 0.1M sodium

cacodylate buffer. After washing, the tissue was stained with 1% osmium tetroxide and 0.5% potassium ferrocyanide in 0.5% sucrose for 1.5 h. The tissues were dehydrated in ascending alcohol series and embedded in epoxy resin. Ultrathin sections of the corpus callosum and dorsal hippocampal commissure were examined with an FEI Morgagni 268 transmission electron microscope at an accelerating voltage of 80 kV. Digital images were acquired with a MegaViewIII camera operated with iTEM software (Olympus Soft Imaging Systems, Germany) and contrast uniformly adjusted with Adobe Photoshop. The average number of myelinated axons in the splenium and dorsal hippocampal commissure were determined from 5–12 (control mice) or 12–27 (cuprizone fed mice) 4400x fields per mouse for each region and are expressed as axons per mm^2. To estimate the number of axonal spheroids per mm^2 in the splenium and dorsal hippocampal commissure, 32–53 overlapping 1800× fields per anatomic area for each mouse (n=2) were automatically photomerged using Adobe Photoshop. Merged pictures were scanned and the number of axonal spheroids/swellings counted. Image J was used to calculate the area of each region, and the results were expressed as axonal spheroids per mm^2.

Statistical analysis

Results are expressed as means ± SEM. Data analysis were conducted using regression analysis, multiple level analysis of variance (ANOVA), and where appropriate Bonferroni's post hoc analysis to determine specific differences between groups. Statistical analyses were performed using GraphPad Prism 4 (GraphPad Software, San Diego, CA).

Results

Cuprizone causes weight loss which subsides after changing the diet to normal chow

We first determined the effects of 5 week 0.2% cuprizone feeding on the overall health of C57BL/6 mice. Throughout the duration of the experiment all mice fed cuprizone appeared clinically normal and did not present with symptoms such as ataxia, seizures or anorexia as observed previously with higher doses (Stidworthy et al., 2003a). Except for an initial reduction of food intake in cuprizone-fed mice on day 2–5 (Supplemental Fig. 2; $p<0.05$), food consumption between mice fed a normal diet and mice fed cuprizone was not different. However, consistent with previous findings (Stidworthy et al., 2003a), mice fed cuprizone lost approximately 10% of their body weight during the first week of intoxication, which was followed by a gradual weight gain during the next 4 weeks. Despite the time-dependent increase in weight, cuprizone-fed mice weighed significantly less than control mice over the course of 5 weeks intoxication (Supplemental Fig. 2; $p<0.001$). Upon returning the cuprizone-fed mice to a normal diet, they gained weight rapidly and after 1 week were no longer different from that of the control mice.

Cuprizone induces demyelination and prominent gliosis in multiple brain regions

We next examined myelin breakdown and gliosis in mice fed a diet with cuprizone for 5 weeks using both histochemical and immunohistochemical approaches. Coronal sections corresponding to the levels of the genu and body of the corpus callosum (1.1 to 0.6 mm from bregma) of cuprizone-fed mice demonstrated nearly complete demyelination of the external capsule (ec) and caudate putamen (cp), as determined by oil red O staining for myelin (Fig. 1A, B). Further examination of these regions by immunohistochemistry revealed a decrease in MBP staining and robust microgliosis in demyelinating regions (Fig. 1 C, D; F–H). In the external capsule there was a parallel increase in the number of $GFAP^+$ astrocytes (Fig. 1E). Additionally, the striatum contained numerous activated microglia localized within and juxtaposed to axon bundles (Fig. 1F–H). Notably, the degree of microgliosis in the caudate putamen was inversely proportionate to the amount of MBP that remained (Fig. 1F–H). Astrocytes with an activated morphology were also present throughout the striatum and in

some cases their processes localized to damaged axon bundles, but to a lesser extent than microglia (not shown).

Oil red O staining of sagittal sections of cuprizone-fed mice revealed demyelination of the cerebellum (Fig. 1I, K). However, demyelination was not evident when the most medial aspects of the cerebellar white matter were examined (Fig. 1J vs. K). Instead, it was only apparent as the sections approached the myelinated fibers of the medial cerebellar nucleus (n=3). The pathology in the cerebellum of cuprizone fed mice was similar to that observed in the external capsule, in that the lack of oil red O stain was associated with decreased MBP immunoreactivity and was coupled with increased microgliosis and astrogliosis within and immediately bordering the lesion (Fig. 1K–N).

Demyelination and gliosis were also prominent features of the cerebral cortex lateral to the external capsule in cuprizone-fed mice (Fig. 1O–Q). Despite the marked reduction in myelin and MBP staining in the cerebral cortex, external capsule and caudate putamen, there was only limited loss of phosphorylated neurofilament immunoreactivity (Fig. 1Q vs. R).

In contrast to the above mentioned pathology, we observed only minor, and in fact variable, differences in the degree of demyelination and gliosis in the callosal body.

The degree of demyelination within the corpus callosum varies anatomically

Serial sections of brain tissue stained with oil red O demonstrated demyelination of the corpus callosum of mice fed cuprizone for 5 weeks when compared to those kept on a normal diet (Fig. 2A vs. B). Remyelination was evident in mice given 2 weeks to recover after 5 weeks of cuprizone feeding (Fig. 2B vs. C). Interestingly, cuprizone administration caused distinct differences in the degree of demyelination within different callosal regions (Fig. 2A vs. B). Specifically, after 5 weeks, there were only minor changes in oil red O intensity in the rostral portion of the corpus callosum (Fig. 2B; bottom left). As noted by others, the changes in this region were not uniform but were patchy in appearance (Fig. 2B) (Stidworthy et al., 2003a). The exception was the superficial portion of the genu of the corpus callosum (gcc), which appeared to be substantially demyelinated at the midline in approximately 80% (4/5) of animals. However, an abrupt and almost complete reduction of myelin was observed in the caudal aspect of the corpus callosum which included the isthmus and splenium as well as the dorsal hippocampal commissure in all (5/5) cuprizone fed mice. The onset of complete demyelination was most apparent when viewed in sagittal sections and was mapped to approximately 0.5 mm caudal to bregma (mean= −0.438; 95% CI= −0.1927 to 0.683; n=5) corresponding to the approximate junction of the callosal body and the isthmus (Fig. 2B). The area of demyelination was accompanied by a vast amount of lipid debris that appeared purple at low magnification in most mice examined (Fig. 2B), and in some instances the oil red O stained myelin debris appeared to be perinuclear, probably indicative of lipid-laden macrophages that were numerous in electron micrographs taken in this region of 5 week cuprizone mice (see below).

Two weeks after cuprizone withdrawal (5+2), myelin was partially restored (Fig. 2A vs. C) and the amount of lipid debris in the caudal regions of the corpus callosum was substantially reduced, although still present in the dorsal hippocampal commissure (Fig. 2C). Indeed, demyelination scores in 5+2 week mice were significantly lower than those of 5 week mice, demonstrating effective remyelination in the affected regions during the 2 week recovery period (Fig. 2D). Importantly, when comparing the demyelination in mice fed cuprizone for 5 weeks with those undergoing remyelination (5+2 week), the scores rostral to −0.8 mm from bregma were not significantly different (Fig. 2D).

Differences in demyelination along the rostral-caudal axis of the corpus callosum were further confirmed by comparing the number of GST-π^+ mature oligodendrocytes in the body (between 0.6 and 0.4 mm from bregma), as well as in the splenium (−0.8 and −1.0 mm caudal to bregma). In the callosal body, the number of GST-π^+ cells per mm^2 in cuprizone fed mice was similar to controls (Fig. 2E, F). In the splenium however, the number of GST-π^+ cells from cuprizone-fed mice were reduced by approximately 90 ± 5.8% (n=3–4) when compared to control samples (Fig. 2E, F). Additionally, the number of GST-π^+ cells differed between the body and the splenium of cuprizone fed mice, but not of control mice (n=3–4; $p<0.01$). Taken together, these results demonstrate that the majority of demyelination in the corpus callosum of mice fed cuprizone for 5 weeks occurs in regions caudal to −0.5 mm from bregma.

Both astrogliosis and microgliosis within the corpus callosum are anatomically distinct

Both astrogliosis and microgliosis are closely correlated with demyelination in the cuprizone model (Hiremath et al., 1998). Therefore, we questioned if the degree of gliosis also varied with respect to bregma. In general, gliosis as determined by GFAP (Fig. 3) and Iba-1 (Fig. 4) immunostaining was most pronounced in mice fed cuprizone for 5 weeks and appeared reduced in mice that recovered for 2 weeks after cuprizone intoxication. This effect was also confirmed in coronal sections, particularity in sections that were anatomically comparable to those that were demyelinated (Fig. 3, 4A–C). In fact, the degree of gliosis within individual animals mirrored demyelination insofar as gliosis was most abundant in the isthmus and splenium as well as the dorsal hippocampal commissure with relatively fewer GFAP$^+$ astrocytes (Fig. 3B; Supplemental Fig. 3) and Iba-1$^+$ microglia (Fig. 4B; Supplemental Fig. 3) in the body of the corpus callosum.

To quantify the extent of gliosis we compared fold change in fluorescence intensity of GFAP or Iba-1 relative to control samples at different anatomical locations. This methodology provided an additional, simple quantitative means to measure gliosis. However, to ensure that this measure was in fact indicative of the level of gliosis, we also determined the number of GFAP$^+$ and Iba-1$^+$ cells per mm^2 and found both approaches yielded consistent results.

GFAP intensity did not differ between normal diet fed controls and cuprizone fed mice within the body of the corpus callosum (0.4 to 0.6 mm from bregma; Fig. 3). However, when the intensity of GFAP was compared within the splenium (−0.8 to −1.0mm from bregma) there were significant differences between groups (Fig. 3D). Specifically, mice kept on a normal diet showed less GFAP intensity than either mice fed cuprizone for 5 weeks ($p<0.001$) or mice allowed to recover for 2 weeks after feeding cuprizone ($p<0.001$). Additionally, mice undergoing remyelination had less GFAP intensity than those treated for 5 weeks (Fig. 3D; $p<0.05$). The same was true when numbers of GFAP$^+$ cells per mm^2 were analyzed (Fig. 3E). In fact, the gliosis as measured by increase in GFAP intensity fold changes was significantly correlated with the number of GFAP$^+$ cells per mm^2 (Fig. 3F). Likewise, no differences in Iba-1 intensity were found between groups when compared at the level of the body of the corpus callosum (between 0.6 to 0.4 mm from the bregma; Fig. 4D). However, Iba-1 intensity was significant higher within regions that mapped to the splenium of the corpus callosum (−0.8 mm from bregma) in the group fed cuprizone for 5 weeks than controls, and withdrawal of cuprizone reduced Iba-1 intensity in caudal regions of the corpus callosum compared to 5 week cuprizone fed mice (Fig. 4D). Analysis of Iba-1$^+$ cells per mm^2 in these regions confirmed the above effect, producing nearly identical results as Iba-1 intensity measurements. As with GFAP intensity, Iba-1 intensity was correlated with Iba-1$^+$ cells per mm^2 (Fig. 4F). Most importantly, both GFAP and Iba-1 intensity and numbers were increased in the caudal aspect of the corpus callosum when compared to the rostral regions of 5 week treated animals, confirming a rostral-caudal gradient in gliosis

(*p*'s<0.05; Fig. 3, 4D&E) that mirrors demyelination. Interestingly, the dorsal hippocampal commissure still appeared to contain elevated numbers of both astrocytes (Fig. 3C) and microglia (Fig. 4C) 2 weeks after cuprizone withdrawal. These results show spatial differences in gliosis within the corpus callosum of mice fed cuprizone for 5 weeks, and indicate differential repair kinetics between the splenium and dorsal hippocampal commissure.

The repair process is delayed in the dorsal hippocampal commissure when compared to the splenium

As mentioned above, the dorsal hippocampal commissure still appeared demyelinated, with increased gliosis when compared to the splenium of the corpus callosum in mice that had been fed cuprizone for 5 weeks and then allowed to recover for 2 weeks (5+2). This raised the possibility that the dorsal hippocampal commissure repairs more slowly than the splenium. We thus examined these regions more closely and measured cells densities, gliosis, and degree of remyelination between groups. Because fluorescence intensity measurements correlated closely with the extent of gliosis as determined by cell counting (Fig. 3&4E), we evaluated astrogliosis, and microgliosis by measuring GFAP and Iba-1 intensity respectively. Within the splenium, the number of cells per mm^2 was increased after 5 weeks on cuprizone, and remained increased after 2 weeks of withdrawal (Fig. 5A). Astrogliosis and microgliosis, determined by measuring GFAP and Iba-1 immunoreactivity respectively, were significantly elevated at 5 weeks, but resolved 2 weeks after cuprizone withdrawal and were no longer significantly different from normal mice (Fig. 5B, C).

As in the splenium, the dorsal hippocampal commissure showed a dramatic increase in cellularity after 5 weeks of cuprizone (Fig. 5D). This increase corresponded to augmented astrogliosis as well as microgliosis (Fig. 5E, F). However, unlike the splenium, astrogliosis and microgliosis remained elevated after 2 weeks of cuprizone withdrawal, and were significantly higher than the control mice (Fig. 5E, F; *p*s<0.05). These data quantitatively confirm our previous observations of substantial ongoing gliosis in the dorsal hippocampal commissure after 2 weeks of cuprizone withdrawal.

Continual gliosis within the dorsal hippocampal commissure may indicate a slower repair process compared to the splenium. In order to determine if this was the case we examined the number of myelinated axons by electron microscopy. After 5 weeks on cuprizone there were substantially fewer myelinated axons in both the splenium (approximately 95.7%; mean of 15–24 fields; n=2) and dorsal hippocampal commissure (approximately 83.9%; mean of 25–27 fields; n=2) when compared to control mice (Fig. 6A, B, C), confirming our conclusions drawn from light microscopy (Fig. 2). Moreover, within these areas of demyelination, there were numerous lipid laden macrophages/microglia (Fig. 6D). Two weeks after cuprizone withdrawal, there was an increase in the number of myelinated axons in the splenium as well as the dorsal hippocampal commissure by approximately 38% (mean of 16–20 fields; n=2) and 17.3% (mean of 12–16 fields; n=2), respectively (Fig. 6B–C). The extent of limited remyelination in the dorsal hippocampal commissure remained similar even 5 weeks after cuprizone cessation (Fig. 6C). Lipid laden macrophages/microglia, which were prevalent during cuprizone intoxication were no longer evident after 2 weeks recovery despite the still elevated microgliosis in the dorsal hippocampal commissure. Thus, the splenium had approximately 20.7% and 37.1% more myelinated axons than did the dorsal hippocampal commissure after 2 and 5 weeks of recovery, respectively (Fig. 6B vs. C; n=2). These findings indicate that only marginal remyelination occurs in the dorsal hippocampal commissure of cuprizone fed mice that have undergone repair for two weeks and 5 weeks and that the splenium of the corpus callosum is more prone to remyelination, thereby a more suitable region for studying cuprizone-induced demyelination and remyelination. The

differences in remyelination between the splenium and dorsal hippocampal commissure may be exploited for identification of molecular machinery required for remyelination.

Axonal damage is more prominent in the dorsal hippocampal commissure compared to the splenium

The variation in remyelination between the dorsal hippocampal commissure and the splenium could attribute to differences in the number of oligodendroglial progenitors migrated to each anatomical site and/or in their capacities to proliferate and differentiate into myelinating cells. In three out of five animals, $NG2^+$ progenitors were found to be more pronounced in the dorsal hippocampal commissure than in splenium (Fig. 7A) while the number of GST-π^+ mature oligodendrocytes did not differ significantly between the two areas (Fig. 7B). This observation indicates that oligodendrocyte progenitor trafficking to the dorsal hippocampal commissure is unlikely to account for the observed differences in remyelination. To determine if the slower repair process in the dorsal hippocampal commissure was associated with axonal pathology, we measured the number of $SMI32^+$ axonal spheroids in these two regions. In mice given five weeks to recover from cuprizone intoxication, $SMI32^+$ immunoreactivity in the corpus callosum exhibited a rostral-caudal gradient pattern that closely mirrored demyelination (not shown). The majority of $SMI32^+$ axonal spheroids were found to be concentrated at the dorsal hippocampal commissure (Fig. 7C, D), where remyelination was also impaired. Electron microscopic analyses confirmed the presence of axonal spheroids/swellings in both areas with the dorsal hippocampal commissure apparently possessing greater number of axonal spheroids/swellings (Fig. 7E, F). Taken together, these data suggest a close relationship between impaired remyelination and increased axonal injury.

Discussion

This study investigated the inconsistencies of demyelination and gliosis occurring within the corpus callosum following standardized cuprizone-induced demyelination. We demonstrate anatomical differences in the extent of demyelination and gliosis within the corpus callosum with the rostral aspects (i.e., genu, and body) being less susceptible to pathological changes than the caudal regions (i.e., isthmus, splenium and dorsal hippocampal commissure). These observations are consistent with results from others (Stidworthy et al., 2003b; Wu et al., 2008; Xie et al., 2010). Importantly, to our knowledge this study is the first to demonstrate that the dorsal hippocampal commissure and splenium differ in the myelin repair process upon cuprizone withdrawal.

Histological examination of mice fed cuprizone showed demyelination in the cerebral cortex, and the external capsule as well as the caudate putamen. As in the corpus callosum the demyelination of the cerebellum showed distinct patterning, with the white matter of the vermis mainly spared (Fig. 1; and (Groebe et al., 2009; Skripuletz et al., 2010). Of interest, much of the caudate putamen was still noticeably demyelinated after two weeks of recovery, while other structures such as the external capsule, cerebral cortex, and corpus callosum showed substantial repair (not shown). As astrocytes have been shown to attract and induce differentiation of oligodendrocyte progenitor cells in this particular model (Patel et al., 2010), it is notable that we did not observe as robust astrogliosis in the caudate putamen, whereas microgliosis was a prominent feature. On the other hand, the dorsal hippocampal commissure demonstrated continual astrogliosis two weeks after cuprizone withdrawal but had delayed remyelination when compared to the splenium.

Several different groups have now shown region-specific differences in the demyelination of the corpus callosum resulting from cuprizone intoxication of C57BL/6 mice (Binder et al., 2008; Stidworthy et al., 2003a; Wu et al., 2008; Yang et al., 2009b, a). In these experiments

the degree of demyelination was predicted to be more severe in the caudal aspects of the callosal structure, a finding later confirmed by MRI and diffusion tensor imaging analysis (Stidworthy et al., 2003a; Wu et al., 2008; Xie et al., 2010) and by the current study. The rostral-caudal differences have been indirectly supported by work involving the spatial organization of the repair processes after cuprizone-induced demyelination as well as by examination of the effects of the immunoregulator GAS6 on demyelination (Binder et al., 2008). Neural progenitor cells injected into the lateral ventricles of cuprizone-demyelinated mice repopulate and repair the superficial aspect of the genu as well as the isthmus and splenium, but not the body of the corpus callosum (Irvine and Blakemore, 2008). Moreover, in a recent study examining the role of CXCR4 in promoting migration of oligodendrocyte progenitors it was found that its ligand, CXCL12, was more abundantly expressed in the caudal aspect of the corpus callosum compared to the most rostral aspects, suggesting an increased reparative process ongoing in the more caudal corpus callosum (Patel et al., 2010).

Our results demonstrate complete demyelination in the caudal regions of the corpus callosum. Importantly, our study provides anatomical parameters for affected callosal regions for use in designing experiments aimed to investigate cuprizone-induced demyelination and the molecular machinery involved in facilitating successful remyelination. These data are particularly relevant when examining coronal sections. Our data strongly suggest that regions caudal to approximately 0.8 mm bregma should be considered when studying remyelination while more rostral regions of the corpus callosum should be avoided as they do not provide adequate separation between groups of mice (Fig. 2). Dual analysis of the dorsal hippocampal commissure and the splenium on sagittal sections may provide valuable insight when examining the effects of treatments on remyelination as these structures appear to repair with a differential kinetics (Fig. 5, 6). A recent study using magnetic resonance diffusion tensor imaging techniques to examine remyelination in cuprizone-fed mice demonstrated the importance of the caudal callosum region in identifying factors involved in remyelination (Tobin et al., 2011). Our findings also suggest that neither the genu nor the body of the corpus callosum are appropriate anatomic locations for the stereotaxic injection of potential therapeutic factors aimed at promoting remyelination, as these locations are not completely demyelinated in the cuprizone model. On the other hand, the callosal body appears to be a more appropriate anatomical area to examine factors that influence demyelination.

Remyelination capacity and the extent of axonal pathology following cuprizone withdrawal vary between the splenium and dorsal hippocampal commissure within individual mice. While the mechanism(s) underlying the regional differences is unknown, it is interesting to note that impaired remyelination and increased axonal pathology were concurrent with persistent gliosis in the dorsal hippocampal commissure despite that there appeared to be more $NG2^+$ progenitors when compared with the splenium. Reactive astrocytes are capable of producing a multitude of factors including trophic factors and cytokines that can either promote or hinder remyelination (Williams et al., 2007). Thus, future experiments designed to elucidate physiological differences between reactive astrocytes in the splenium versus the dorsal hippocampal commissure may provide insight into the differences in remyelination processes between these two regions.

The differential sensitivity to cuprizone-induced demyelination along the corpus callosum may have a few implications. As the largest compact white-matter structure in the brain, the corpus callosum is anatomically divided into five separate regions, from rostral to caudal, the lamina rostralis, the genu, the body, the isthmus, and the splenium (Raybaud, 2010). The corpus callosum can also be subdivided into two physiologically separate regions. While the genu and body are responsible for the commissural transfer of myelinated axons originating from the prefrontal cortex, premotor cortex, primary motor cortex, and supplemental motor

area, the splenium and dorsal hippocampal commissure are involved in the transfer of sensory information from the posterior parietal cortex temporal lobe and occipital lobe (Raybaud, 2010). The isthmus, which is located at the junction of the fornix and callosal body between the septum pellucidum and hippocampal commissure, contains fibers from the motor strip, somato-sensory strip and the primary auditory cortex (Raybaud, 2010). As such, it can be predicted that mice undergoing cuprizone-induced demyelination might experience more difficulty with sensory modalities rather than motor function. This is consistent with the fact that cuprizone mice do not have obvious clinical signs (Ludwin, 1978). However, this interpretation must be made with caution as we and others have demonstrated demyelination in other structures, including the caudate putamen and the cerebellum (Groebe et al., 2009; Pott et al., 2009; Skripuletz et al., 2010), which may in part contribute to the decreased performance of cuprizone mice in the rotarod test as observed by several groups.

Toxin induced neuropathies have been known for a long time to also differentially affect specific regions of the brain. For example, isonicotinic acid hydrazide given to Peking ducks caused severe demyelination of the cerebellar medulla, white matter folia and deep cerebellar nuclei, while the medullary layer of occipital lobe, tectothalamic tract and cerebellar peduncles are less affected (Carlton and Kreutzberg, 1966). Additionally, hexachlorophene toxicosis and triethyltin can cause specific demyelination pattering and gliosis with similarities to that of described for cuprizone (Poppenga et al., 1990). In humans, inhalation of heroin vapor, industrial solvents, methanol misuse, alcohol abuse and nutritional deficiency can cause distinct patterns of demyelination with characteristic appearance upon imaging (Smith and Smirniotopoulos; Smith and Smirniotopoulos, 2010). The corpus callosum is suspected to be affected in almost all MS patients (Gean-Marton et al., 1991). Unlike the regional distribution following cuprizone intoxication, diffusion tensor image mapping studies of MS patients have, however, demonstrated the callosal body and isthmus as being most affected areas while the genu and splenium the least (Ge et al., 2004; Lou et al., 2009; Ozturk et al.). Therefore, while it is peculiar that the isthmus, splenium and dorsal hippocampal commissure are more susceptible to cuprizone-induced demyelination when compared to the genu and body, this is not necessarily surprising as different demyelinating diseases with different etiologies show distinctive pathological patterning.

In conclusion, we have demonstrated rostral-caudal differences in demyelination and gliosis within the corpus callosum structure following cuprizone intoxication. We have mapped the location for gliosis and demyelination of the corpus callosum to approximately 0.5 mm caudal to bregma, and have demonstrated substantial differences in remyelination of these regions following cuprizone withdrawal. Together, these data provide guidance for the design of studies aimed at uncovering the mechanisms involved in demyelination and remyelination using this animal model.

Supplementary Material

Refer to Web version on PubMed Central for supplementary material.

Acknowledgments

This work was supported by NIH grant R01NS060017, by the research grant RG3975 from the National Multiple Sclerosis Society, and by the start-up funds from Texas A&M University. We thank Dr. Regina Armstrong for sharing her cuprizone feeding protocol, Ms. Lin Bustamante for technical support, and Dr. Ross Payne for his help with electron microscopy.

References

Arnett HA, Mason J, Marino M, Suzuki K, Matsushima GK, Ting JP. TNF alpha promotes proliferation of oligodendrocyte progenitors and remyelination. Nat Neurosci. 2001; 4:1116–1122. [PubMed: 11600888]

Bando Y, Takakusaki K, Ito S, Terayama R, Kashiwayanagi M, Yoshida S. Differential changes in axonal conduction following CNS demyelination in two mouse models. Eur J Neurosci. 2008; 28:1731–1742. [PubMed: 18973589]

Barnett MH, Prineas JW. Relapsing and remitting multiple sclerosis: pathology of the newly forming lesion. Ann Neurol. 2004; 55:458–468. [PubMed: 15048884]

Binder MD, Cate HS, Prieto AL, Kemper D, Butzkueven H, Gresle MM, Cipriani T, Jokubaitis VG, Carmeliet P, Kilpatrick TJ. Gas6 deficiency increases oligodendrocyte loss and microglial activation in response to cuprizone-induced demyelination. J Neurosci. 2008; 28:5195–5206. [PubMed: 18480276]

Blakemore WF. Observations on oligodendrocyte degeneration, the resolution of status spongiosus and remyelination in cuprizone intoxication in mice. J Neurocytol. 1972; 1:413–426. [PubMed: 8530973]

Blakemore WF. Demyelination of the superior cerebellar peduncle in the mouse induced by cuprizone. J Neurol Sci. 1973; 20:63–72. [PubMed: 4744511]

Breij EC, Brink BP, Veerhuis R, van den Berg C, Vloet R, Yan R, Dijkstra CD, van der Valk P, Bo L. Homogeneity of active demyelinating lesions in established multiple sclerosis. Ann Neurol. 2008; 63:16–25. [PubMed: 18232012]

Carlton WW, Kreutzberg G. Isonicotinic acid hydrazide-induced spongy degeneration of the white matter in the brains of Pekin ducks. Am J Pathol. 1966; 48:91–105. [PubMed: 5902838]

Compston A, Coles A. Multiple sclerosis. Lancet. 2008; 372:1502–1517. [PubMed: 18970977]

Duncan ID, Brower A, Kondo Y, Curlee JF Jr, Schultz RD. Extensive remyelination of the CNS leads to functional recovery. Proc Natl Acad Sci U S A. 2009; 106:6832–6836. [PubMed: 19342494]

Franklin, BJ.; Paxinos, G. The mouse brain in stereotaxic coordinates. 3. Academic Press; New York: 2008.

Ge Y, Law M, Johnson G, Herbert J, Babb JS, Mannon LJ, Grossman RI. Preferential occult injury of corpus callosum in multiple sclerosis measured by diffusion tensor imaging. J Magn Reson Imaging. 2004; 20:1–7. [PubMed: 15221802]

Gean-Marton AD, Vezina LG, Marton KI, Stimac GK, Peyster RG, Taveras JM, Davis KR. Abnormal corpus callosum: a sensitive and specific indicator of multiple sclerosis. Radiology. 1991; 180:215–221. [PubMed: 2052698]

Groebe A, Clarner T, Baumgartner W, Dang J, Beyer C, Kipp M. Cuprizone treatment induces distinct demyelination, astrocytosis, and microglia cell invasion or proliferation in the mouse cerebellum. Cerebellum. 2009; 8:163–174. [PubMed: 19259754]

Gudi V, Moharregh-Khiabani D, Skripuletz T, Koutsoudaki PN, Kotsiari A, Skuljec J, Trebst C, Stangel M. Regional differences between grey and white matter in cuprizone induced demyelination. Brain Res. 2009; 1283:127–138. [PubMed: 19524552]

Hiremath MM, Saito Y, Knapp GW, Ting JP, Suzuki K, Matsushima GK. Microglial/macrophage accumulation during cuprizone-induced demyelination in C57BL/6 mice. J Neuroimmunol. 1998; 92:38–49. [PubMed: 9916878]

Irvine KA, Blakemore WF. Remyelination protects axons from demyelination-associated axon degeneration. Brain. 2008; 131:1464–1477. [PubMed: 18490361]

Kipp M, Clarner T, Dang J, Copray S, Beyer C. The cuprizone animal model: new insights into an old story. Acta Neuropathol. 2009; 118:723–736. [PubMed: 19763593]

Koutsoudaki PN, Skripuletz T, Gudi V, Moharregh-Khiabani D, Hildebrandt H, Trebst C, Stangel M. Demyelination of the hippocampus is prominent in the cuprizone model. Neurosci Lett. 2009; 451:83–88. [PubMed: 19084049]

Linares D, Taconis M, Mana P, Correcha M, Fordham S, Staykova M, Willenborg DO. Neuronal nitric oxide synthase plays a key role in CNS demyelination. J Neurosci. 2006; 26:12672–12681. [PubMed: 17151270]

Liu L, Belkadi A, Darnall L, Hu T, Drescher C, Cotleur AC, Padovani-Claudio D, He T, Choi K, Lane TE, Miller RH, Ransohoff RM. CXCR2-positive neutrophils are essential for cuprizone-induced demyelination: relevance to multiple sclerosis. Nat Neurosci. 2010; 13:319–326. [PubMed: 20154684]

Lou X, Jiang W, Ma L, Ma N, Cai Y, Huang D, Wong EH. Lower fractional anisotropy at the anterior body of the normal-appearing corpus callosum in multiple sclerosis versus symptomatic carotid occlusion. Neuroradiology. 2009; 51:557–561. [PubMed: 19504090]

Lucchinetti C, Bruck W, Parisi J, Scheithauer B, Rodriguez M, Lassmann H. Heterogeneity of multiple sclerosis lesions: implications for the pathogenesis of demyelination. Ann Neurol. 2000; 47:707–717. [PubMed: 10852536]

Ludwin SK. Central nervous system demyelination and remyelination in the mouse: an ultrastructural study of cuprizone toxicity. Lab Invest. 1978; 39:597–612. [PubMed: 739762]

Matsushima GK, Morell P. The neurotoxicant, cuprizone, as a model to study demyelination and remyelination in the central nervous system. Brain Pathol. 2001; 11:107–116. [PubMed: 11145196]

Mi S, Miller RH, Tang W, Lee X, Hu B, Wu W, Zhang Y, Shields CB, Miklasz S, Shea D, Mason J, Franklin RJ, Ji B, Shao Z, Chedotal A, Bernard F, Roulois A, Xu J, Jung V, Pepinsky B. Promotion of central nervous system remyelination by induced differentiation of oligodendrocyte precursor cells. Ann Neurol. 2009; 65:304–315. [PubMed: 19334062]

Ozturk A, Smith SA, Gordon-Lipkin EM, Harrison DM, Shiee N, Pham DL, Caffo BS, Calabresi PA, Reich DS. MRI of the corpus callosum in multiple sclerosis: association with disability. Mult Scler. 16:166–177. [PubMed: 20142309]

Pasquini LA, Calatayud CA, Bertone Una AL, Millet V, Pasquini JM, Soto EF. The neurotoxic effect of cuprizone on oligodendrocytes depends on the presence of pro-inflammatory cytokines secreted by microglia. Neurochem Res. 2007; 32:279–292. [PubMed: 17063394]

Patel JR, McCandless EE, Dorsey D, Klein RS. CXCR4 promotes differentiation of oligodendrocyte progenitors and remyelination. Proc Natl Acad Sci U S A. 2010; 107:11062–11067. [PubMed: 20534485]

Plant SR, Arnett HA, Ting JP. Astroglial-derived lymphotoxin-alpha exacerbates inflammation and demyelination, but not remyelination. Glia. 2005; 49:1–14. [PubMed: 15382206]

Poppenga RH, Trapp AL, Braselton WE, Louden CG, Gumbs JM, Dalley JB. Hexachlorophene toxicosis in a litter of Doberman pinschers. J Vet Diagn Invest. 1990; 2:129–131. [PubMed: 2094434]

Pott F, Gingele S, Clarner T, Dang J, Baumgartner W, Beyer C, Kipp M. Cuprizone effect on myelination, astrogliosis and microglia attraction in the mouse basal ganglia. Brain Res. 2009; 1305:137–149. [PubMed: 19799876]

Raybaud C. The corpus callosum, the other great forebrain commissures, and the septum pellucidum: anatomy, development, and malformation. Neuroradiology. 2010; 52:447–477. [PubMed: 20422408]

Skripuletz T, Bussmann JH, Gudi V, Koutsoudaki PN, Pul R, Moharregh-Khiabani D, Lindner M, Stangel M. Cerebellar cortical demyelination in the murine cuprizone model. Brain Pathol. 2010; 20:301–312. [PubMed: 19371354]

Skripuletz T, Lindner M, Kotsiari A, Garde N, Fokuhl J, Linsmeier F, Trebst C, Stangel M. Cortical demyelination is prominent in the murine cuprizone model and is strain-dependent. Am J Pathol. 2008; 172:1053–1061. [PubMed: 18349131]

Smith AB, Smirniotopoulos JG. Imaging evaluation of demyelinating processes of the central nervous system. Postgrad Med J. 86:218–229. [PubMed: 20354045]

Stidworthy MF, Genoud S, Suter U, Mantei N, Franklin RJ. Quantifying the early stages of remyelination following cuprizone-induced demyelination. Brain Pathol. 2003a; 13:329–339. [PubMed: 12946022]

Suzuki K, Kikkawa Y. Status spongiosus of CNS and hepatic changes induced by cuprizone (biscyclohexanone oxalyldihydrazone). Am J Pathol. 1969; 54:307–325. [PubMed: 5765567]

Taylor LC, Gilmore W, Matsushima GK. SJL mice exposed to cuprizone intoxication reveal strain and gender pattern differences in demyelination. Brain Pathol. 2009; 19:467–479. [PubMed: 19016742]

Taylor LC, Gilmore W, Ting JP, Matsushima GK. Cuprizone induces similar demyelination in male and female C57BL/6 mice and results in disruption of the estrous cycle. J Neurosci Res. 2010; 88:391–402. [PubMed: 19746424]

Tobin JE, Xie M, Le TQ, Song S-K, Armstrong RC. Reduced Axonopathy and Enhanced Remyelination After Chronic Demyelination in Fibroblast Growth Factor 2 (Fgf2)-Null Mice: Differential Detection With Diffusion Tensor Imaging. Journal of Neuropathology & Experimental Neurology. 2011; 70:157–165. 110.1097/NEN.1090b1013e31820937e31820934. [PubMed: 21343885]

Williams A, Piaton G, Lubetzki C. Astrocytes - Friends or foes in multiple sclerosis? Glia. 2007; 55:1300–1312. [PubMed: 17626262]

Wu QZ, Yang Q, Cate HS, Kemper D, Binder M, Wang HX, Fang K, Quick MJ, Marriott M, Kilpatrick TJ, Egan GF. MRI identification of the rostral-caudal pattern of pathology within the corpus callosum in the cuprizone mouse model. J Magn Reson Imaging. 2008; 27:446–453. [PubMed: 17968901]

Xie M, Tobin JE, Budde MD, Chen CI, Trinkaus K, Cross AH, McDaniel DP, Song SK, Armstrong RC. Rostrocaudal analysis of corpus callosum demyelination and axon damage across disease stages refines diffusion tensor imaging correlations with pathological features. J Neuropathol Exp Neurol. 2010; 69:704–716. [PubMed: 20535036]

Yang HJ, Wang H, Zhang Y, Xiao L, Clough RW, Browning R, Li XM, Xu H. Region-specific susceptibilities to cuprizone-induced lesions in the mouse forebrain: Implications for the pathophysiology of schizophrenia. Brain Research. 2009a; 1270:121–130. [PubMed: 19306847]

Highlights

- We examine cuprizone-induced demyelination and remyelination in the corpus callosum
- Mapping rostral-caudal regional differences in demyelination and gliosis
- The caudal corpus callosum structure shows reliable demyelination and remyelination
- Kinetics for myelin repair differs between splenium and dorsal hippocampal commissure

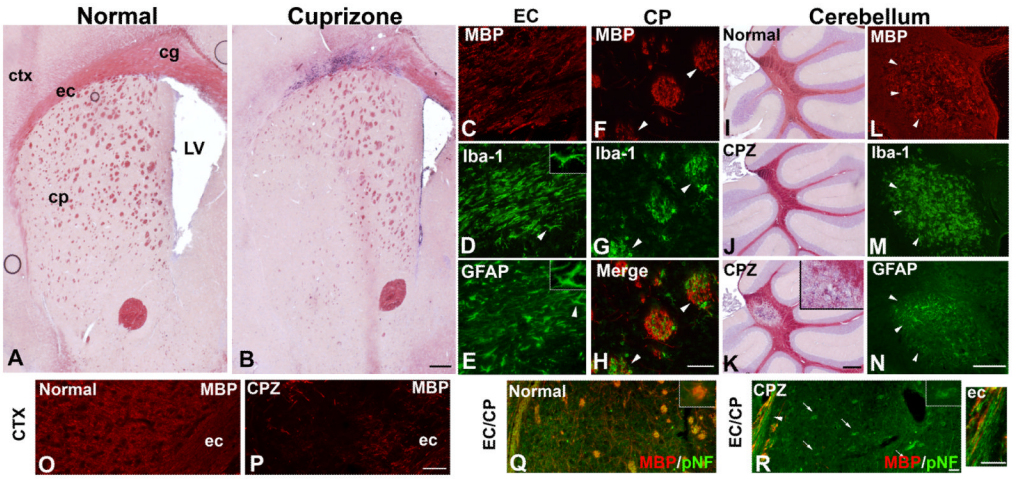

Figure 1. Demyelination and gliosis occur in multiple brain structures after 5 weeks of cuprizone feeding

Mice were kept on a normal diet or fed 0.2% cuprizone (CPZ) for 5 weeks. **A&B,** Coronal sections at the level of the genu (1.1 mm bregma) were stained for myelin with oil red O. Comparisons between normal **(A)** and CPZ fed **(B)** mice showed decreased oil red O intensity in the cortex (ctx), cingulated gyrus (cg), external capsule (ec) and caudate putamen (cp) of CPZ mice. LV is lateral ventricle. **C–E**, Immunohistochemical staining of the external capsule using specific antibodies to MBP **(C)**, Iba-1 **(D)**, and GFAP **(E)**. Individual Iba-1$^+$ and GFAP$^+$ cells (arrows) are depicted at a higher magnification in the inserts. **F–H,** In the caudate putamen of cuprizone fed mice, microglia were localized to demyelinating axon bundles (arrows) as determined by immunostaining. **I–K,** Sagittal sections of the cerebellum at the level of the medial nuclei of a normal **(I)** or at the midline of CPZ fed **(J)** mouse demonstrated conserved myelin by oil red O staining. Same mouse as in J showed reduced oil red O intensity at the level of the medial nucleus **(K)**. Insert is lesion edge magnified 5X. **L–N,** Closer examination of cerebellar pathology by immunohistochemistry showed decreased MBP staining **(**arrows, **L)** as well as increased Iba-1$^+$ microglia **(**arrows, **M)** and GFAP$^+$ astrocytes **(**arrows, **N)** within and on edge of lesions. **O&P,** Representative pictures demonstrating MBP staining in the cortex and external capsule (ec) of a normal **(O)** and cuprizone fed mouse **(P). Q&R,** The external capsule and caudate putamen showing reduced MBP staining (red) but relatively normal phosphorylated neurofilament (pNF) distribution (green) in cuprizone fed mouse **(R)** vs. control mouse **(Q)**. Inserts in Q&R are of axon bundles magnified 3X. Scale bars, **A, B, I–K,** 200 μm; **C–H, L–P,** 50 μm; **Q–R,** 25 μm. Pictures are representative of 3–4 mice per group at each location and condition.

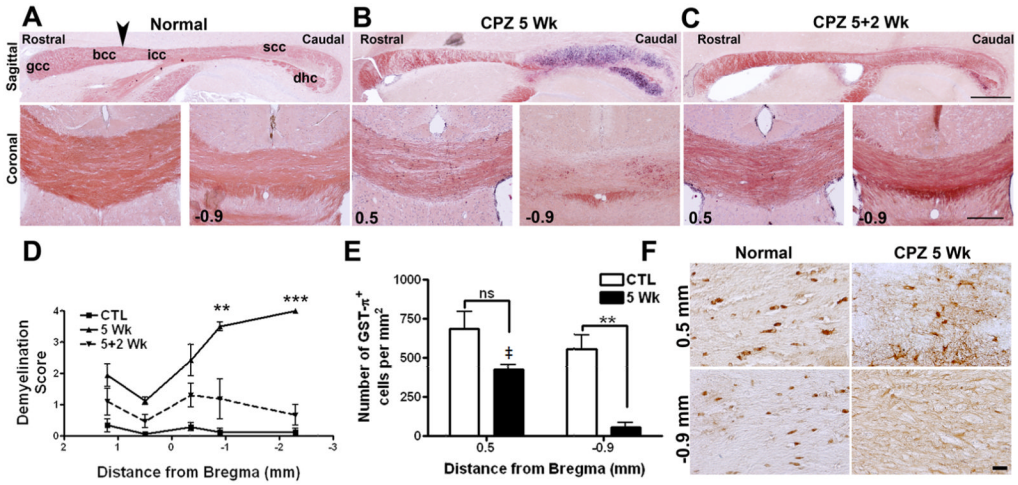

Figure 2. Demyelination is distinct in specific callosal regions after cuprizone intoxication

Mice were fed a normal diet or one containing 0.2% cuprizone for 5 weeks (5 wk) to induce demyelination. In some mice cuprizone was withdrawn after 5 weeks and the diet returned to normal chow for 2 week to allow recovery (5+2 wk). **A–C**, Serial sagittal and coronal sections were stained for myelin with oil red O. Sagittal sections showing the genu (gcc), body (bcc), isthmus (icc), and splenium of the corpus callosum (scc) as well as the dorsal hippocampal commissure (dhc) of a normal **(A)**, 5 week treated **(B)** or recovered mouse (5+2; **C**). Scale bar = 500 μm. Coronal sections of normal **(A)**, cuprizone **(B)** and cuprizone + recovery **(C)** groups corresponding to approximately 0.5 and −0.9 mm from the bregma. Scale bar = 200 μm. **D**, Average demyelination scores with respect to the bregma. Data are means ± SEM from n=3–5 animals. **E–F**, The number of GST-π^+ mature oligodendrocytes per mm^2 at 0.5 ± 0.1 mm and −0.9 ± 0.1 mm to the bregma **(E)** and representative pictures **(F)**. Results are representative from n=3–4 animals. **, $p<0.01$. ‡, $p<0.01$ between 0.5 and −0.9mm.

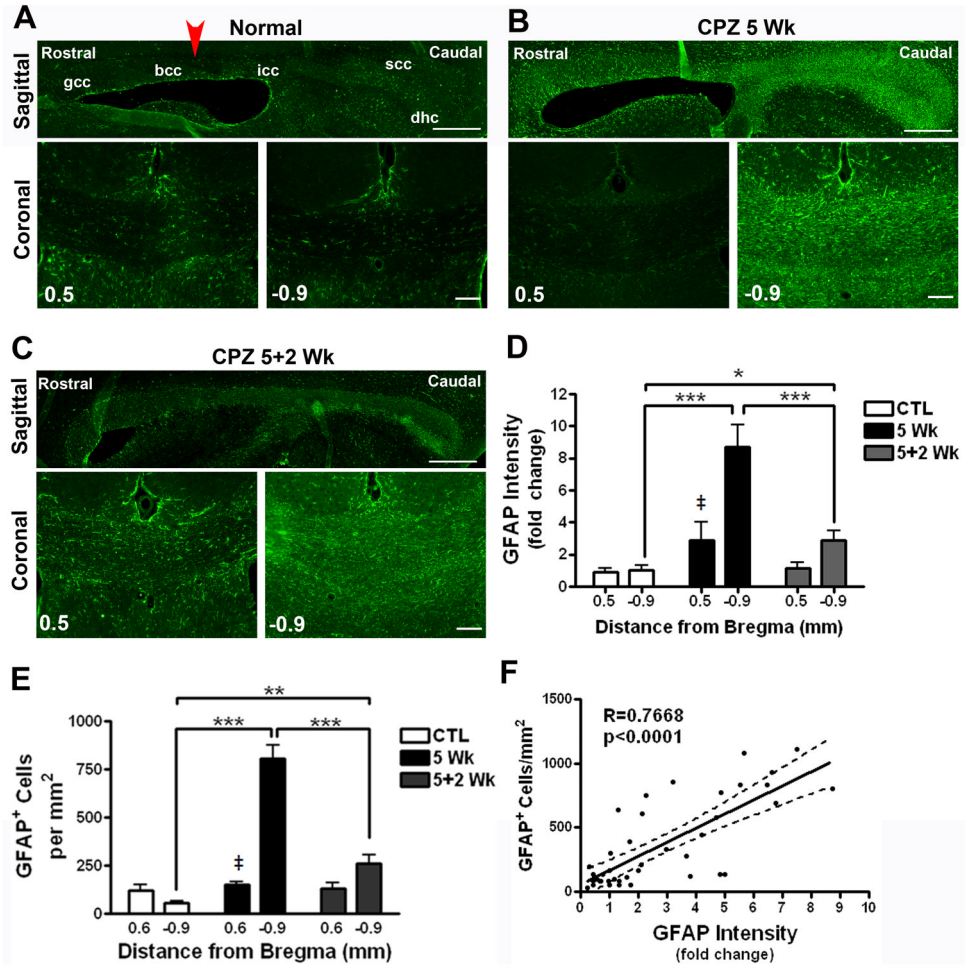

Figure 3. Degree of astrogliosis following cuprizone intoxication mirrors demyelination

Mice were treated as in Fig. 3. **A–C**, Serial sagittal and coronal sections at indicate anatomical locations were stained for GFAP$^+$ astrocytes by immunohistochemistry. Bregma represented by arrow. Scale bars for sagittal sections = 500 μm, coronal sections = 200 μm. **D&E**, Astrogliosis quantified by measuring fold change in GFAP fluorescence intensity **(D)** and by counting cell number of nucleated cells **(E)** and graphed with respect to bregma. **F,** Regression analysis showing a significant correlation between GFAP fluorescence intensity analysis and GFAP$^+$ cell number analysis. Data are means ± SEM; n=3–5. *, $p<0.05$; **, $p<0.01$; ***, $p<0.001$ when compared to controls. ‡, $p \leq 0.05$ between 0.5 and −0.9mm.

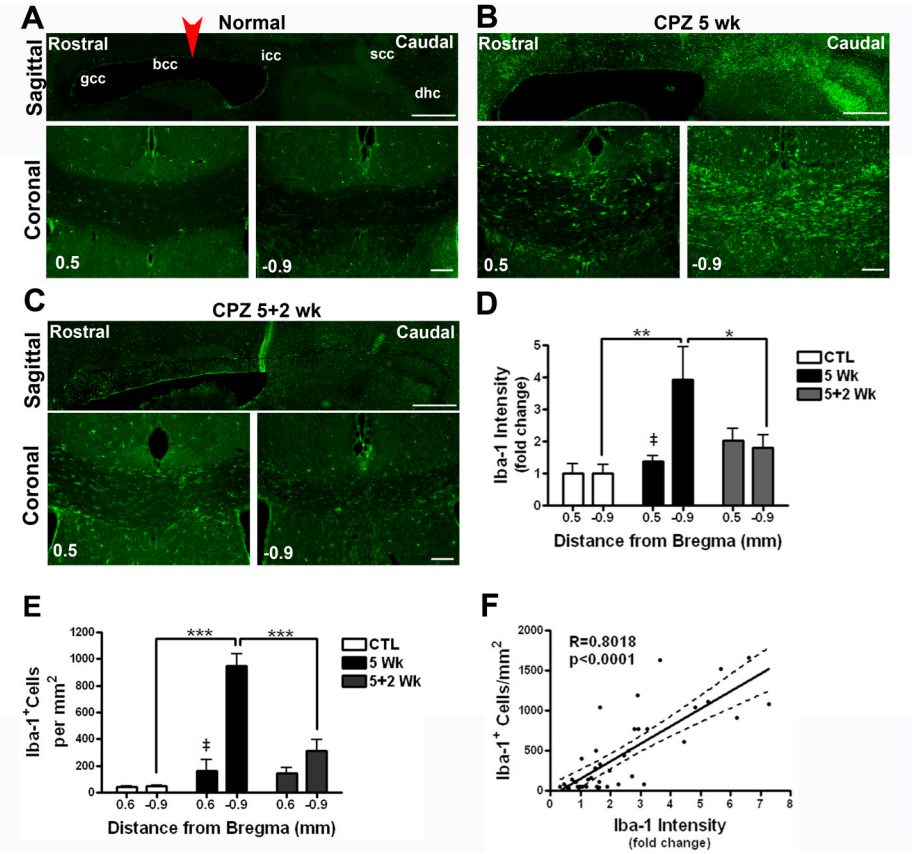

Figure 4. Microgliosis following cuprizone intoxication correlates with demyelination

Mice were treated as in Fig. 3. **A–C**, Serial sagittal and coronal sections at indicate anatomical locations were stained for Iba-1$^+$ microglia by immunohistochemistry. Bregma represented by arrow. Scale bars for sagittal sections = 500 μm, coronal sections = 200 μm. **D&E**, Microgliosis quantified by measuring fold change in Iba-1 fluorescence intensity **(D)** and by counting cell number of nucleated cells **(E)** and graphed with respect to bregma. **F,** Regression analysis showing a significant correlation between Iba-1 fluorescence intensity analysis and Iba-1$^+$ cell number analysis. Data are means ± SEM; n=4–5. *, $p<0.05$; **, $p<0.01$; ***, $p<0.001$ when compared to controls. ‡, $p \leq 0.05$ between 0.5 and −0.9mm.

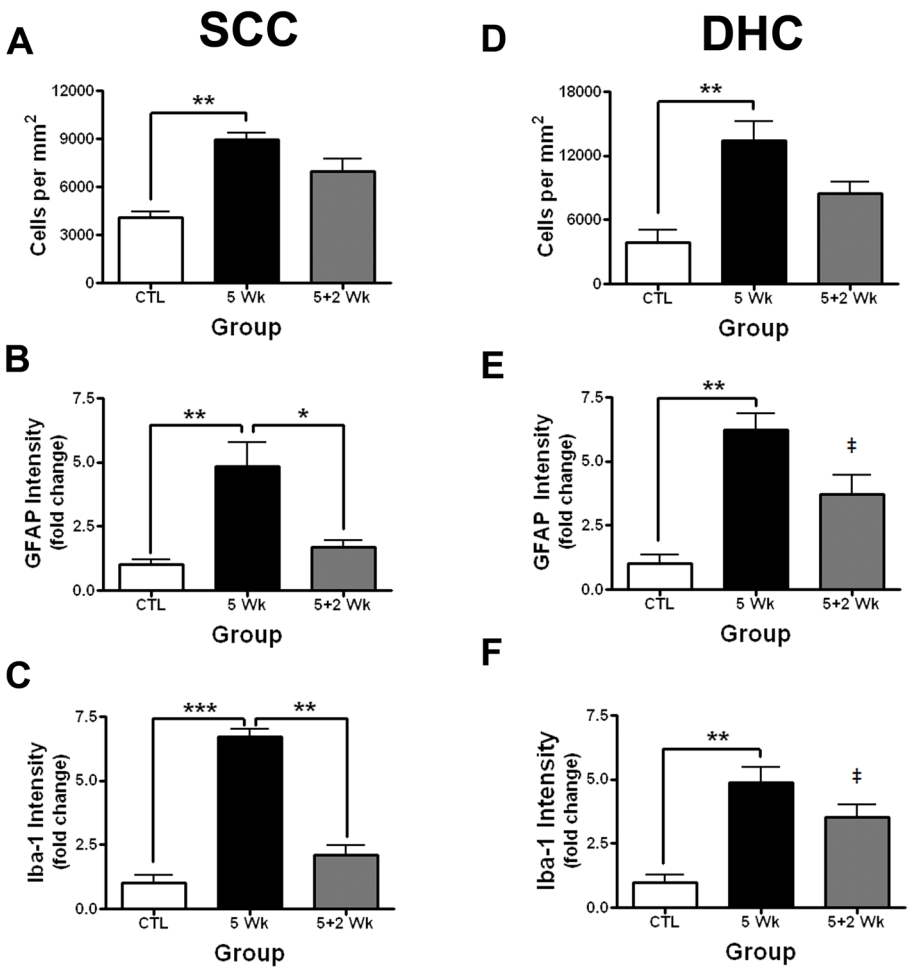

Figure 5. Gliosis differs between the splenium, and dorsal hippocampal commissure after 2 weeks of recovery

The extent of gliosis was quantified in the splenium corpus callosum (SCC; **A–C**), and dorsal hippocampal commissure (DHC; **D–F**) of mice undergoing demyelination (5 week; 5wk) or remyelination (5+2 week; 5+2 wk) and compared to those kept on a normal diet (CTL). Total cell number per mm^2 was increased after 5 weeks of cuprizone in the SCC (**A**) and DHC (**B**) an effect that diminished in the DHC after 2 weeks of withdrawal. **B–C,** Both GFAP and Iba-1 intensity were increased relative to controls in the SCC after 5 weeks on cuprizone. After 2 weeks of recovery the amount of gliosis was lower at 5 weeks and did not differ from control mice. **E–F,** GFAP and Iba-1 intensity were increased in the DHC to the same extent as the SCC (**B, C vs. E, F**) after 5 weeks of cuprizone. However, unlike in the SCC, this increase persisted in the DHC after 2 weeks of cuprizone withdrawal. Results are means ± SEM; n=3. *, $p<0.05$; **, $p<0.01$; ***, $p<0.001$. ‡, $p<0.05$ compared to CTL.

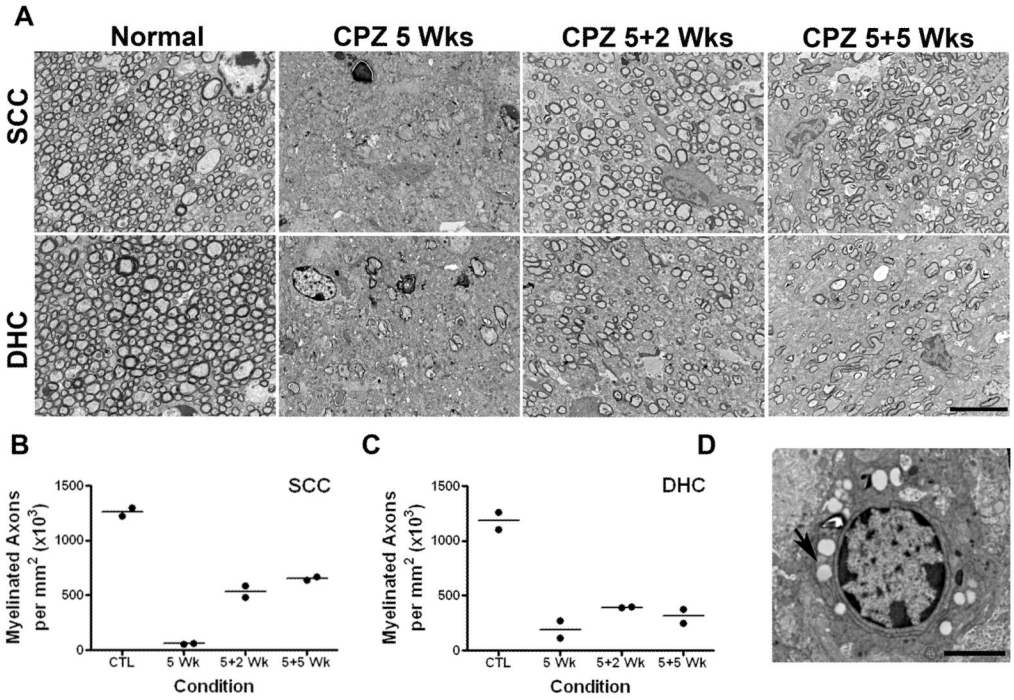

Figure 6. The repair process is slower in the dorsal hippocampal commissure compared to the splenium corpus callosum after 2 weeks of recovery from cuprizone

Mice were fed a normal diet (CTL) or one containing 0.2% cuprizone for 5 weeks to induce demyelination (5 wk). In some mice cuprizone was withdrawn after 5 weeks and the diet returned to normal chow for 2 weeks (5+2 wk) or 5 weeks (5+5 wk) to allow recovery. **A,** Representative electron micrographs showing myelinated axons in the splenium corpus callosum (SCC; top) and dorsal hippocampal commissure (DHC; bottom) of normal, 5, 5+2, and 5+5 week mice. Scale bar = 5μm. **B–C,** The number of myelinated axons per mm^2 was determined for the SCC (B) as well as the DHC (C). **D,** Representative micrograph showing microglia with multiple lipid droplets within the cytosol (arrow) taken of mouse at 5 weeks post cuprizone. Scale bar = 2.5 μm. Results in B and C represent the mean number of axons per mm^2 derived from 5–12 4400x fields (control mice) or 12–27 4400x fields (cuprizone fed mice) for each mouse; n=2.

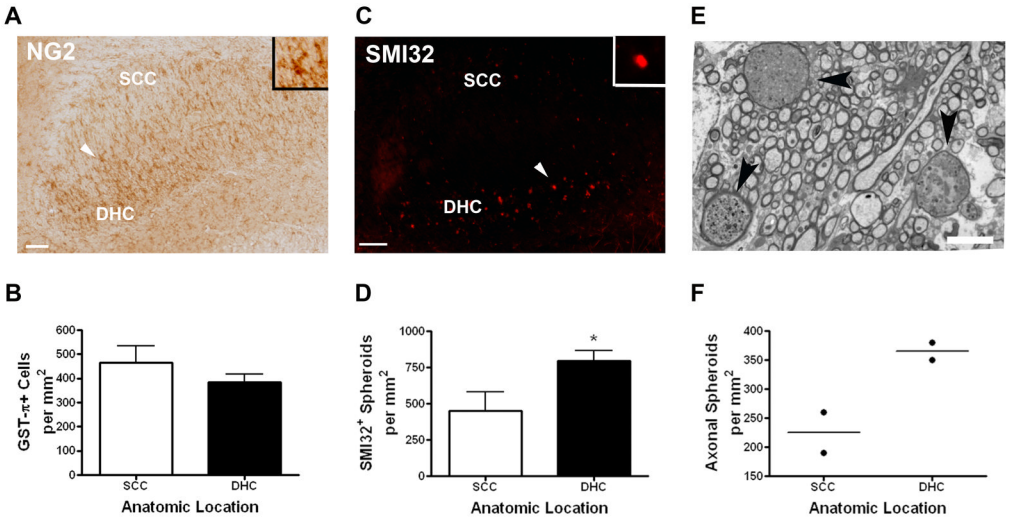

Figure 7. Increased axonal dystrophy in the dorsal hippocampal commissure compared to the splenium

Mice were fed cuprizone for 5 weeks and allowed to recovery for four (IHC) to five weeks (EM). **A,** Representative picture showing NG2 immunoreactivity in the splenium (SCC) and the dorsal hippocampal commissure (DHC). Arrow depicts a $NG2^+$ cell magnified in the insert. Scale bar = 50μm. **B,** GST-π^+ mature oligodendrocytes per mm^2 in the SCC and DHC. Results are means ± SEM; n=5. **C–D,** Increased axonal dystrophy as determined by SMI32 immunoreactivity in the dorsal hippocampal commissure when compared to the splenium. Scale bar=50 μm. Result represents mean ± SEM; n=5. *, $p<0.05$. **E,** Representative electron micrograph showing 3 axonal spheroids/swellings in the DHC (arrows). Scale bar =5 μm. **F,** The number of axonal spheroids/swellings estimated from 32–53 1800× fields for each mouse per area; n=2.